SYNCHROTRON X-RAY DIFFRACTOMETRY AND IMAGING OF STRAINS AND DEFECTS IN ICOSAHEDRAL QUASICRYSTAL GRAINS

Joseph Gastaldi, Thomas Schenk, L Mancini, Holger Klein, Juergen Haertwig, S Agliozzo, Jose Baruchel, Marc de Boissieu

SYNCHROTRON X-RAY DIFFRACTOMETRY AND IMAGING OF STRAINS AND DEFECTS IN ICOSAHEDRAL QUASICRYSTAL GRAINS

Journal:	*Philosophical Magazine & Philosophical Magazine Letters*
Manuscript ID:	TPHM-06-Mar-0077.R1
Journal Selection:	Philosophical Magazine
Date Submitted by the Author:	26-May-2006
Complete List of Authors:	Gastaldi, Joseph; CRMCN, Campus de Luminy Schenk, Thomas; Laboratoire de Physique des Matériaux, Ecole des Mines de Nancy Mancini, L; Sincrotrone Trieste SCpA, SYRMEP Group Klein, Holger; Laboratoire de Cristallographie, CNRS Haertwig, Juergen; ESRF Agliozzo, S; ISI Baruchel, Jose; European Synchrotron Radiation Facility; European Synchrotron Radiation Facility de Boissieu, Marc; LTPCM UMR CNRS 5614; LTPCM UMR CNRS 5614
Keywords:	defects, quasicrystals, strain
Keywords (user supplied):	

SYNCHROTRON X-RAY DIFFRACTOMETRY AND IMAGING OF STRAINS AND DEFECTS IN ICOSAHEDRAL QUASICRYSTAL GRAINS

J. GASTALDI*†, T. SCHENK‡, L. MANCINI¶, H. KLEIN§, J. HÄRTWIGg#, S. AGLIOZZO ǁ, J. BARUCHEL# and M. DE BOISSIEU£

† CRMCN-CNRS, Campus de Luminy, case 913, 13288 Marseille Cedex 9, France,
‡ LPM, Ecole des Mines de Nancy, Parc de Saurupt, CS 14234, 54 042 Nancy Cedex, France
¶ SYRMEP Group, Sincrotrone Trieste S.C.p.A., 34012 Basovizza (Trieste), Italy
§ CNRS, Laboratoire de Cristallographie, BP 16, 38042 Grenoble, France
# ESRF, BP 220, Grenoble, France
ǁ ISI, Villa Gualino, Viale Settimio Severo 65, 10133 Torino, Italy,
£ LTPCM/ENSEEG - Domaine Universitaire, BP 7538402 St Martin d'Hères Cedex, France

ABSTRACT

In order to better understand the long range propagation of quasicrystalline order as well as quasicrystal stability, it is important to know if defects are generated in the quasicrystal grains during their growth. Previously, we studied the degree of perfection of about ten icosahedral quasicrystal grains of various alloys (Al-Pd-Mn, Al-Cu-Fe, Zn-Mg-Y), as grown or annealed, and we disclosed that some of them were much more perfect than the others. In this work we have concentrated on another slice of such a grain of the Al-Pd-Mn alloy. Similarly, we have performed an extensive Synchrotron X-ray Topographic investigation of strain and defects in this grain, combined with Phase Contrast Radiography and High Resolution X-ray Diffraction examinations. Very few two-lobes contrasts associated to pores and no loop-shaped contrasts were observed on X-ray topographs, this time, but straight line segments and band contrasts have been identified. Line segments could be considered as the result of the climbing of polygonal dislocation loops as those observed, by TEM, by Caillard *et al*. This would indicate that most of strains and defects observed in quasicrystal grains, at room temperature, are the result of stresses (external and internal) acting after growth.

1. Introduction:

Whether the quasicrystal growth has to incorporate defects to ensure the stability of the quasicrystal lattice, or not, remain a challenge which set the supporters of the energy influence [1] against those of the entropy effect [2].

It has been reported that some quasicrystal grains are probably highly perfect since they give rise to anomalous X-ray transmission [3], but this assumption has not been confirmed by direct observations of the amount of strains and defects contained in these grains by using X-ray topography [4] [5].

Otherwise, investigations of defects by Transmission Electron Microscopy (TEM) in many as-grown and annealed grains have concluded to a minimum dislocation density of about 10^{10} to 10^{11} m/m^3 [4], which is substantial.

* Corresponding author. Email: gastaldi@crmcn.univ-mrs.fr

Deleted: ON

Deleted: A "HIGHLY PERFECT"

Deleted: ASSESED¶ BY SYNCHROTRON X-RAY DIFFRACTOMETRY AND IMAGING

Deleted: After having

Deleted: are

Deleted: [2] [3]

Deleted: ,

Deleted: a grain

Deleted: [10]

Deleted: [13]

Deleted: us they

Deleted: , remain

Deleted: s

Deleted: 1

Deleted: 2

Deleted: 3

Deleted: 10^6

Deleted: 10^7

Deleted: c

Deleted: c

Deleted: consequent

Deleted: †

Comparing to what is known for crystals, such a dislocation density is a limit below which it is difficult to detect these defects by TEM. Besides it has been determined that it does not disturb too much the anomalous X-ray transmission [7] [8]. Therefore, there is a need of further investigations using X-ray topography which is a technique appropriate to the characterization of defects at a low density level. Indeed, this technique allows to image defects in relatively thick grains (0.2 – 1 mm) precisely when they are not too numerous (dislocation density < 10^8 m/m^3) [9]. Likewise it is possible to get contrasts from strain fields (up to a long range of about a few tens of micrometers) of individual defects the appearance of which is tightly related to the dynamical interaction of X-rays inside the grain lattice and are thereby highly indicative of the degree of lattice perfection. Using the X-ray beam delivered by the third generation synchrotron improves on one hand the spatial resolution of the X-ray topographs owing to the smallness of the source of these synchrotrons and on the other hand introduces additional useful phase contrasts generated by the high transverse coherence of this beam [10].

Previously we have demonstrated that this technique is suitable for quasicrystals [9] and studied the degree of perfection of about ten icosahedral quasicrystal grains of various alloys (Al-Pd-Mn, Al-Cu-Fe, Zn-Mg-Y). Therefore we disclosed that some of them are much more perfect than the others [4] [5]. In this work we have concentrated on another slice of such a grain of the Al-Pd-Mn alloy. Similarly, we have performed an extensive Synchrotron X-ray Topographic investigation of defects in this grain, combined with Phase Contrast Radiography and High Resolution X-ray Diffraction examinations. Very few two-lobes contrasts associated to pores and no loop-shaped contrasts [12] were observed on X-ray topographs, this time, but straight line segments and band contrasts have been identified and attributed to events occurring after the growth process.

2. Experiments:

The most perfect grain of a polygrained Al-Pd-Mn quasicrystalline sample, having a size of about 2x2x0.3mm^3, was selected according to the narrow (less than 10 arc second) Full Width at Half Maximum (FWHM) of the rocking Curves (RC) recorded from some of its areas, (50x50) μm^2 large, by synchrotron X-ray High Resolution Diffraction (HRD). This grain was investigated further, by this technique, varying the X-ray energy in order to detect anomalous X-ray transmission. In addition, Phase Contrast Radiographs and X-ray Topographs were exposed simultaneously, so as to image defects and their surrounding strain field which are accountable of both the enlargement of RCs and the disturbance of the anomalous X-ray transmission. The thin sample (0.3 mm thick) was prepared by the AMES Laboratory. It was cut out of a quasicrystal, grown by the Bridgman technique using a mother alloy of the composition $Al_{70}Pd_{20}Mn_{10}$. Most of the X-ray experiments were carried out at the ID19 station of the European Synchrotron Radiation Facility (ESRF) in Grenoble (France)[†].

This beamline, dedicated to X-ray imaging and HRD, is characterized by a very long source-to-sample distance (150 m) and a small angular source size seen from a point of the sample (0.1 – 1 μrad) which ensure a high geometrical resolution on X-ray topographs (0.1 μm). The small source size (≅ 100μm) combined to the long source-to-sample distance

[†]Complementary experiments were performed at the Italian synchrotron, ELETTRA, in Trieste, in similar conditions.

Deleted: 5
Deleted: 6
Deleted: r
Deleted: t
Deleted: as
Deleted: it
Deleted:
Deleted: 10^4
Deleted: c
Deleted: c
Deleted: 7
Deleted: 8
Deleted: 7
Deleted: 2
Deleted: 3
Deleted: 10
Deleted: ,
Deleted: in
Deleted: an ingot, of composition $Al_{70}Pd_{20}Mn_{10}$
Deleted: at the AMES Laboratory
Deleted: Main
Deleted: *
Deleted: spatial
Deleted: a
Deleted: L

provides on the other hand the large transverse coherence length (≅ 40µm for λ=0.516Å) necessary for the observation of phase contrasts on the radiographs. The beam was monochromatized by two perfect Si crystals diffracting in the (+,-) non-dispersive setting. The spectral width was $\Delta\lambda/\lambda \cong 10^{-4}$. The X-ray topographs were recorded either on films (Kodak SR) or on plates (Ilford L4 25µm) whereas phase-contrast radiographs were captured either on High Resolution films (Kodak SR) or by a CCD based camera developed at the ESRF and named FReLoN (Fast Read Out Low Noise) [13].

'[Insert figure 1 about here]'

3. Results:

Figure 1 is an X-ray topograph, which shows the spatial distribution of strain and defects inside the whole volume of the selected grain. Black, grey and white regions can be seen in the image. They correspond to different parts of the grain which are continuously misoriented as proved by the necessity to rock the grain along the Bragg peak by an amount of 0.05° for their complete imaging. Thereby, lattice curvatures with a radius of about 2 m for the entire grain and of about 0.5 m for a region of (50x50) µm^2 were evidenced. Besides, two-lobes, linear and band contrasts, respectively marked TL, L_i and B_i in Figure 1, can be distinguished in these regions. The few two-lobes contrasts present are associated to the pores visible in phase contrast radiographs, as previously shown [12]. As for linear and band contrasts, they are certainly related to defects located in the volume of the grain as indicated by the section topographs in Figure 2b which are true optical cuts of the sample at the level of the arrows in figure 2a.

'[Insert figure 2 about here]'

This is suggested, in this figure, by the line contrast L*i* and band contrasts B*i* which are spreading in the middle of the section topograph image instead of limiting themselves to the sides. By the way one has to notice that there are no more Pendellösung fringes in this section topograph than in all other ones we recorded, either from other places in the grain or using other diffraction vectors. The only fringe sets we disclosed in section topographs were in restricted parts of the grain volume and were probably related to fault sequences like local condensation of phasons (Figure 3).

'[Insert figure 3 about here]'

'[Insert figure 4 about here]'

Otherwise, anomalous X-ray transmission was detected, measured and imaged (Figure 4), in this grain, as it was observed in a previous one of the same family [4]. Moreover very narrow rocking curves were recorded from some of its (50x50) µm^2 areas and FWHM down to 0.0009° were measured (Figure 5). It was also noticed that displacing the incident X-ray beam 50 µm side-away change the FWHM value up to 100%.

'[Insert figure 5 about here]'

'[Insert figure 6 about here]'

We tried to determine the directions and the displacement vectors of lines L*i* as well as those of band B*i*, respectively labelled $\mathbf{l}L_i$, $\mathbf{d}L_i$ for L_i and $\mathbf{l}B_i$, $\mathbf{d}B_i$ for B_i. To this intent, we recorded X-ray topographs using twelve different diffraction vectors $\mathbf{g}_j$ (Figure 6). In both cases we faced with the same difficulty, i.e. it was impossible to recognize lines L_i and bands B_i in all of the various X-ray topographs so obtained, impeding us to characterize fully each of these two defects. For the determination of the line directions $\mathbf{l}L_i$ and $\mathbf{l}B_i$, we need to analyze three X-ray topographs, recorded with three different diffraction vectors $\mathbf{g}_i$ in which defects are visible. This is required in order to dispose of at least three different projection images

Deleted:

Deleted: on-line detector that consists of a scintillator converting X-ray into visible light, coupled to a CCD

Deleted: with a microscope objective

Deleted: call

Deleted: 11

Deleted: In

Deleted: is

Deleted: present

Deleted: which has been selected

Deleted: also

Deleted: F

Deleted: T

Deleted: few

Deleted: 10

Deleted: and both are not so numerous in this grain

Deleted:

Deleted: 2

Deleted:

Deleted: d

Deleted: which

Deleted: ed

Deleted: ,

Deleted: , are required

allowing to reconstruct the inclination of the defects in the grain volume. This was possible only for lines L_1 because they appeared grouped in a family unlike the others (Figure 1) and thereby were easier to find again. It was determined that the direction of these lines was along the [-1/-1 0/1 0/0] two-fold axis inclined at about 75 degrees relatively to the normal of the grain surface which is along one of the other two-fold axes ([0/0 0/0 0/1]) (Figure 6). As for the determination of the displacement vectors $\mathbf{d}L_1$ associated to these defects (Burgers' vectors $\mathbf{b}L_1$ in case of dislocations) the application of the invisibility criterion $\mathbf{g}_j.\mathbf{d}L_i = \mathbf{0}$ was somewhat unsuccessful as discussed later. Again we get only some information for lines L_1. As they were visible in reflections $\mathbf{g}_j$ oriented along [-1/0 0/-1 0/0], this means that the displacement vector $\mathbf{d}L_1$ is not in the direction of the line $\mathbf{l}L_1$ [-1/-1 0/1 0/0] which is perpendicular, i.e. L_1 are not of the pure screw type. As for the determination of the exact direction of $\mathbf{d}L_1$, some ambiguity is remaining because lines L_1 are not visible in too many reflections (at least 6:…).

Deleted: ¶
Deleted: ¶
Deleted: by
Deleted: hat
Deleted:

4. Discussion:

Unlike the previous one we investigated [4][5], this new "highly perfect" Al-Pd-Mn quasicrystal grain allowed us to distinguish, clearly, individual defects in X-ray topographs. However, a complete characterization of all of them was not possible (determination of $\mathbf{l}L_i$, $\mathbf{d}L_i$ …) despite their low density. This density was estimated to be of about 10^8 - 10^9 m/m^3 from the various X-ray topographs we recorded from the same region as that of figure 2a. Although this value is indeed lower than the density of defects in the previously studied "highly perfect" Al-Pd-Mn grain [4][5] and much lower than that reported by TEM observations [4], it remains close to the upper limit of the possibilities of defect characterization by X-ray topography [9]. Therefore, as this technique is very sensitive to low strains [9] and allows to image defects by their strain fields extending up to a few tens of micrometres, one can guess that when the number of defects is as large as 10^8 - 10^9 m/m^3, some overlapping strain fields can disturb the visibility of the corresponding contrasts and leads to the failure of the invisibility criterion $\mathbf{g}_j.\mathbf{d}L_i = \mathbf{0}$. Moreover, it can also be supposed that the observed lattice curvatures, although they have a large radius (0.5m – 2m), will increase this effect. Nevertheless, as long as straight defects L_i and bands B_i (up to more than 100 μm) are clearly distinguished in many X-ray topographs and even if it has been impossible to fully characterize them, they can be tentatively compared to dislocations and phason faults observed by TEM [14][15][16][17].

L_i defects are looking like the straight dislocation segments reported by Caillard *et al.* as well in as-grown grains [15] as in deformed ones at high temperature [17]. They are much longer (≅ 100 μm instead of ≅ 0.1 μm) but this is certainly due to the difference of thickness between our sample (300μm) and those investigated by these authors who used TEM. Despite that they did not give any indication, it can be thought that the thickness of their samples was at most a few 0.1 μm which results in an equivalent ratio: defect length/ thickness of the sample. Besides, L_i defects can be considered as likewise oriented as those observed by Caillard *et al.*, provided we suppose that the identification of L_1 defects to one of the same axis, we made in section III, can be extended to all of them. Carrying on this hypothesis is the fact that two L_i defects are sometimes linked, making an angle close to that of two two-fold directions (L_1L_2, L_1L_3, in figure 1)[‡]. Pursuing the comparison, for instance,

Deleted: 2
Deleted: 3
Deleted: 10^4
Deleted: 10^5
Deleted: c
Deleted: c
Deleted: 2
Deleted: 3
Deleted: of defects
Deleted: 7
Deleted: 7
Deleted: 10^4
Deleted: 10^5
Deleted: c
Deleted: c
Deleted: 12
Deleted: 13
Deleted: 14
Deleted: 15
Deleted: 13
Deleted: 15
Deleted: such
Deleted: **
Deleted: by

[‡] As it can be estimated directly, by comparing the topograph in figure 1 to the stereographic projection along the incident X-ray beam (figure 6), neglecting the Bragg angle and bearing in mind that L_1 is oriented along the [-1/-1 0/1 0/0] two fold axis

with the discussion of the ability of these defects to climb, a property of quasicrystal dislocations revealed by Caillard *et al*. [14], is difficult because we have been unable to determine their displacement vectors.

Nevertheless, one can guess that they are the result of climbing defects (dislocations?) generated by stress centres existing in as-grown quasicrystal grains as it has been suggested also by Caillard, *et al*. [15]. Similarly we could suppose that L_i defects arise from the climbing of polygonal loops which intersect the sample external surfaces and leave dislocation segments inside the quasicrystal grain. Stress centres could be pores and precipitates as we previously evidenced and discussed [12] [18]. Indeed, during the annealing of quasicrystal single grains, we observed defects with loop-shaped contrasts enlarging while precipitates were growing and pores shrinking. Despite these defects had not a segmented aspect on X-ray topographs [11] [12], it can yet be supposed that their loop-shaped contrast, which were difficult to analyse [18], results from the sum of the unresolved strain fields of concentric polygonal dislocation loops like those observed by TEM by Caillard *et al*. [15]. This consideration would corroborate one of the two hypothesis we brought forward in 1997 after having also identified by TEM analysis straight dislocation segments inside the same sample in which we precisely observed loop-shaped contrasts by synchrotron X-ray topography [19] [20]. The climbing of such giant defects, over a large distance, has already been observed in crystals during "in situ" studies, carried out by synchrotron X-ray topography, of the growth of recrystallized pure aluminium grains. It was then clearly seen that long screw dislocations, emitted by moving grain boundaries, climbed immediately into segmented helical dislocations [21]. Afterward, the pitches and diameters of these helical dislocations increased rapidly until they disappeared when reaching the external surfaces of the samples, leaving thereby mixed dislocations segments inside the grains [22]. It was thus calculated that only a very small vacancy supersaturation is necessary to allow climbing of such long dislocations (1.000005 for a 1mm long screw dislocation at 500°C [23]), a condition which is easily fulfilled, either during very slow cooling [23] or annealing at constant temperature, owing to the thermal fluctuations arising from the furnace temperature controller. In our case of interest, an estimation of both the supersaturation of vacancies needed and that standing in quasicrystal grains during solidification, annealing or cooling, can be made likewise using values of ΔH_f, b, μ, … given in the literature for AlPdMn quasicrystals (see Appendices 1 and 2). Similar results are thus obtained which sustain our hypothesis. The vacancy supersaturation $S_{(T)}$ could be high enough during solidification (the temperature gradient is of about 10 to 30K/cm at the level of the interface) as well as the after-growth cooling, to activate Bardeen-Herring sources and generate large dislocation loops like those we observe together with Caillard *et al*.. Moreover, in electron microscopy experiments of Caillard *et al*.[13] both the gradient and fluctuations of temperature inside the electron microscope furnace might be greater than in ours, which is consistent with their observations of loops of smaller size [a ΔT of 30-35K is sufficient to activate a Bardeen-Herring source of a few 0.1μm length (Appendices 1and 2)]. Our observations are also corroborated, insofar as the better temperature control of our furnace is compatible with the growth of larger loops [the activity of Bardeen-Herring sources of about a few 10 μm long can be triggered by a ΔT in the 0.1-2K range (Appendices 1and 2)]. Therefore, it can be supposed that the L_i defects are the remnants of climbing concentric polygonal dislocation loops, like those reported from TEM studies [15]. These loops appearing as loop shaped defects in X-ray topographs owing to the poor spatial resolution inherent to this technique, especially when defects are too numerous [9]. Nonetheless, if L_i defects were partially resolved it is certainly due to the improvement of the perfection of the investigated quasicrystal grain, during the after-growth annealing [5]. This is corroborated on one hand by the unusual very narrow rocking curves we recorded from this grain (section III) and on the

Deleted: commenting
Deleted: for example
Deleted: 12
Deleted: , precisely,
Deleted: 13
Deleted: 10
Deleted: 16
Deleted: We i
Deleted:
Deleted:
Deleted: defects
Deleted:
Deleted: ,
Deleted: , during the annealing of quasicrystal single grains
Deleted: loop shaped defects
Deleted:
Deleted: 9
Deleted: 10
Deleted: s
Deleted: 16
Deleted: s
Deleted: 13
Deleted: , by TEM,
Deleted:
Deleted: defec
Deleted: t
Deleted: 17
Deleted: 18
Deleted: , carried out by synchrotron X-ray topography
Deleted: 19
Deleted: 20
Deleted: 21
Deleted: .
Deleted: A
Deleted: 21
Deleted: imagin
Deleted: 13
Deleted: 7
Deleted: 3

other hand by the very few number of pores observed in the corresponding X-ray topographs (Figures 1 and 2) because pores are known to be numerous in the volume of as-grown grains [12] and to shrink during annealing [24].

As for contrasts B_i , they are certainly not associated to the double contrasts of L_i defects because they appeared so, in all X-ray topographs where they were visible, independently of the diffraction vector $\mathbf{g}_i$ we used. Moreover their contrast line are much larger (Figures 1 and 2) than those of L_i defects. Therefore B_i contrasts are probably linked to a different type of defect. They could be thought to limit some planar defects (phason walls, stacking fault [14]) for example, because some fringe sets were disclosed in some section X-ray topographs (Figure 4) despite the insufficient degree of perfection of the studied quasicrystal grain (section III).

Accordingly, it appears that this AlPdMn icosahedral quasicrystal grain, though being the most perfect one we have ever studied up to now (section III), contains still a lot of strains and defects. Furthermore, the synchrotron X-ray topographic investigation of this grain seems to indicate that they are the results of stresses, either external (thermal stresses…) or internal (pores…) acting after the growth of grains. This phenomenon is well known in the case of the growth of both semiconductor [25] and metallic crystals for which it was demonstrated that the dislocation density (length) was increased by climbing, thanks to the activity of Bardeen-Herring or Amelinckx-Bontinck sources[¶] during cooling [22] [26]. We already put forward this proposal [5] [11] and Caillard *et al*. have recently emphasized the feasibility of such a dislocation mechanism in quasicrystals [17]. Therefore one can wonder whether strains and defects are mainly generated in quasicrystals after growth or during the growth process itself. For metallic crystals the situation is clear: no or very few strains and defects are induced in these grains by the moving growth interfaces either during recrystallization or solidification as it was proven by "in situ" synchrotron X-ray topography studies [19] [27] [28] [29]. No such studies have been carried out, up to now, during the growth of quasicrystals but we have started one which is in progress. The challenge is not only to determine when strains and defects are generated in quasicrystal grains but also to assess if they are constituent elements of the quasicrystal lattice and hence intrinsic to the icosahedral structure. This could help to better understand as well the long range propagation of the quasicrystalline order as the quasicrystal stability.

5. Conclusion:

The main results of this extensive Synchrotron X-ray Topographic investigation, combined with Phase Contrast Radiography and High Resolution X-ray Diffraction examinations, of defects in a newly selected perfect grain, are:

- very few two-lobes contrasts associated to pores and no loop-shaped contrasts [12] were observed in this case on X-ray topographs, but straight line segments and band contrasts together with some fringe patterns, which are not Pendellösung fringes, have been identified. These observations confirm that real quasicrystals are far from being "highly perfect" (no lattice curvature, very few dislocations: much less than 10^7 m/m^3) as it was believed when their ability to transmit anomalously X-ray was evidenced.
- line segments which have been difficult to fully characterize and were supposed oriented along two fold axes, could be considered as the result of the climbing of polygonal dislocation loops as those observed, by TEM, by Caillard *et al*. [15]. Thus they would

[¶] Bardeen-Herring [30] sources are like Frank-Read sources (anchored edge-dislocation segments) but are acting in the plane perpendicular to the gliding plane (climbing plane) instead inside the gliding plane itself. Amelinckx-Bontinck [31] sources differ from the Bardeen-Herring sources by the starting dislocation segment which has a mixed character with a strong screw component.

Deleted: 10
Deleted: 22
Deleted: n other
Deleted: 12
Deleted: crystals
Deleted: 23
Deleted: 20
Deleted: 24
Deleted: 3
Deleted: 9
Deleted: 15
Deleted: 17
Deleted: 25
Deleted: 26
Deleted: 27
Deleted: constitutive
Deleted: in order to
Deleted: constituents
Deleted: It will
Deleted: ,
Deleted: combined with Phase Contrast Radiography and High Resolution X-ray Diffraction examinations,
Deleted: 10
Deleted: , this time
Deleted: 10^3
Deleted: c
Deleted: c
Deleted: 13
Deleted: 28
Deleted: 29
Deleted:

indicate that most of the strains and defects observed in quasicrystal grains at room temperature are the result of stresses (external and internal) acting after growth. This hypothesis has to be checked by an "in situ" observation of the quasicrystal growth.

Acknowledgments:

The authors are very grateful to S. W. Kycia for having kindly provided them with this new "highly perfect" grain, to M. Kleman, V. Dmitrienko for helpful discussions and to the technical staffs of the ESRF and ELETTRA for their assistance.

Appendix:

A1: vacancy supersaturation $S_{(T)}$ which could run in an AlPdMn quasicrystal during solidification or annealing:

$$S_{(T)} = C_T / C_{(e)T}$$

C_T = actual concentration of vacancies in the grain at a temperature T,
$C_{(e)T}$ = concentration of vacancies given by the thermal equilibrium at the same temperature T,

$$S_{(T)} = \exp [- \Delta H_f (1/ T_1 - 1/ T_2)/ k] \quad T_1 > T_2 \qquad [32]$$

ΔH_f = vacancy formation enthalpy, k = Boltzman constant, T_1,T_2= temperatures.

By taking the value ΔH_f = 1.22 x 10^{-19} Joule given for AlPdMn by Sato *et al.* [33], T_1 = 1133K and k = 1.38 x 10^{-23}, we have calculated the vacancy supersaturation $S_{(T)}$ prevailing in an AlPdMn quasicrystal for 5 values of the temperature gradient $\Delta T = T_1 - T_2$ which could exist, either close to the interface during solidification or in the grain during annealing:

ΔT	0.1	2	10	20	35
$S_{(T)}$	1.0021	1.0425	1.2315	1.5167	2.1200

A2: vacancy supersaturation $S_{(T)}$ necessary for the activation of Bardeen-Herring sources in an AlPdMn quasicrystal:

In order that an edge dislocation segment in a vacancy environment, pined at its two extremities, acts as a Bardeen-Herring source of loop dislocations, the osmotic force induced by the vacancy supersaturation $S_{(T)}$ must exceed the dislocation line-tension force. Thus:

$$S_{(T)} \geq \exp \{ (\mu b v_a kT / 2\pi L(1- \nu)) (\ln \alpha/ 1.8b) \} \qquad [28]$$

By taking the atomic volume $v_a = b^3$ (b = Burgers' vector module), the coefficient α = 4, an average value of the shear modulus μ = 60 GPa according to the Tanaka *et al.* measurements [34], (1- ν) = 0.75 [15] and a mean value of $b_{//}$ = 035 nm [17], we have estimated the vacancy supersaturation necessary to activate Bardeen-Herring sources, in an AlPdMn quasicrystal, at a temperature close to the melting temperature, 1133 K, during its growth by solidification, for 3 lengths L of the edge dislocation segment.

L	0.1µm	1µm	30µm

$S_{(T)}$	2.2012	1.1130	1.0050

References:

[1] Steinhart, P.J., and Ostlund, S., *The Physics of Quasicrystals,* World Scientific Press, Singapore (1987).

[2] D. Shechtman, and I. Blecht, *Metall. Trans. A*, 16, 1005 (1985).

[3] S.W. Kycia, A.I. Goldman, T.A. Lograsso, D.W. Delaney, D. Black, M. Sutton, E. Dufresne, R. Bruning and B. Rodricks, *Phys. Rev. B*, **48**, 3544 (1993).

[4] J. Härtwig, S. Agliozzo, J. Baruchel, R. Colella, M. de Boissieu, J. Gastaldi, H. Klein, L. Mancini and J. Wang, *J. of Phys. D: Applied Phys.* **34** A103-A108 (2001).

[5] J. Gastaldi, S. Agliozzo, A. Letoublon, J. Wang, L. Mancini, H. Klein, J. Härtwig, J. Baruchel, I.R. Fisher, T. Sato, A.P. Tsai and M. de Boissieu, *Phil. Mag*. **83**, 1 (2003).

[6] M. Wollgarten and K. Urban, *Lectures on Quasicrystals,* edited by F. Hippert and D. Gratias, (Les Editions de Physique Publishing), p535 (1994).

[7] B.W. Batterman, *J. Appl. Phys.* , **30**, 508 (1959).

[8] B. Nøst, B.C. Larson and F.W. Young, *J. Phys. Stat. Sol,* , **11**, 263 (1972).

[9] A. Authier A., *NATO ASI Series*, Series B: Vol. 357, *X-ray and Neutron Dynamical Diffraction: theory and applications*, Erice, Italy, edited by A. Authier, S. Lagomarsino and B.K. Tanner (New York: Plenum Press, 1996), p. 1.

[10] P. Cloetens, M. Pateyron-Salomé, J.Y. Buffière, G. Peix, J. Baruchel, F. Peyrin and M. Schlenker, *J. Appl. Phys.*, **81**, 5878 (1997).

[11] J. Gastaldi, E. Reinier, C. Jourdan, G. Grange, A. Quivy and M. Boudard, *Phil. Mag. Lett.*, **72**, 311 (1995).

[12] L. Mancini, E. Reinier, P. Cloetens, J. Gastaldi, J. Härtwig, M. Schlenker and J. Baruchel, *Phil. Mag. A,* **78** 1175 (1998).

[13] J.C. Labiche, J. Segura-Puchades, D. van Brussel and J.P. Moy, ESRF *Newslett.* **25** 41 (1996).

[14] D. Caillard, G. Vanderschaeve, L. Bresson and D. Gratias, *Phil. Mag. A,* **80** 237 (2000).

[15] D. Caillard, C. Roucau, L. Bresson and D. Gratias, *Acta Materialia*, **50**, 4499 (2002).

[16] F. Mompiou, L. Bresson, P. Cordier and D. Caillard, *Phil. Mag.*, **83**, 3133 (2003).

[17] F. Mompiou, D. Caillard, and M. Feuerbacher, *Phil. Mag.*, **84**, 2777 (2004).

[18] S. Agliozzo, *Thesis*, University Joseph Fourier, Grenoble, France (2002).

Deleted: 1987,
Formatted: Font: Times New Roman
Deleted: D.
Deleted:
Deleted: , I.
Deleted: 1985,
Deleted: ,
Deleted: ¶
Formatted: Font: Italic
Formatted: Font: Times New Roman, Not Bold
Formatted: Font: Times New Roman
Deleted: 1
Deleted: 2
Deleted: 3
Deleted: 4
Deleted: 5
Deleted: 6
Deleted: 7
Deleted: 8
Deleted: 9
Deleted: 10
Formatted: Font: Times New Roman
Deleted: 11
Deleted: 12
Deleted: 13
Deleted: 14
Deleted: 15
Deleted: 16

[17] E. Reinier, J. Gastaldi, L. Mancini, J. Härtwig, J. Baruchel, and N. Baluc, *Proceedings of the 6th International Conference on Quasicrystals,* Tokyo May 1997, edited by Takeuchi S. and Fujiwara T., (World Scientific, 1998), p.417.

[19] E. Reinier, *Thesis*, University Paul Cézanne, Marseille, France (1998).

[20] J. Gastaldi, C. Jourdan and G. Grange, *Phil. Mag. A,* **57**, 971 (1988).

[22] J. Gastaldi and C. Jourdan, *J. of Crystal growth*, **35**, 17 (1976).

[23] J. Gastaldi, *Thesis*, University Paul Cézanne, Marseille, France (1975).

[24] S. Agliozzo, J. Gastaldi, H. Klein, J. Härtwig, J. Baruchel and E. Brunello, *Physical Review B*, **69**,144204 (2004).

[25] E. Billig, *Proc. Roy. Soc.,* **A35**, 37 (1956).

[26] B. Nøst, G. Sorensen and E. Nes, *J. of Crystal growth*, **1**, 149 (1967).

[27] J. Gastaldi, C. Jourdan and G. Grange, *Colloque de Physique, Supplément au n° 1*, **51**, C1 405 (1990).

[28] G. Grange, J. Gastaldi and C. Jourdan, *J. Appl Phys.,* **62**, 1202 (1987).

[29] G. Grange, C. Jourdan, J. Gastaldi and B. Billia, B., *J. de Phys. III*, **4**, 293 (1994).

[30] J. Bardeen and C. Herring, *Imperfections in nearly perfect crystals*, Wiley New York, 261 (1952).

[31] S. Amelinckx, W. Bontinck, W. Dekeyser and F. Seitz, *Phil. Mag.*, **2**, 355 (1957).

[32] J.P. Hirth, J. Lothe, *Theory of dislocation*, Mc Graw-Hill, New York (1968).

[33] K. Sato, F. Baier, A.A. Rempel, W. Sprengel and H.-E. Schaefer, *Phys. Rev. B* **68** 214203 (2003).

[34] K. Tanaka, Y. Mitarail and M. Koiwa, *Phil. Mag. A,* **73**, 1715 (1996).

Deleted: 18

Deleted: 19

Deleted: 20

Deleted: 21

Deleted: 22

Deleted: 23

Deleted: 24

Deleted: 25

Deleted: 26

Deleted: 27

Deleted: 28

Deleted: 29

Deleted: 30

Deleted: 31

Deleted: 32

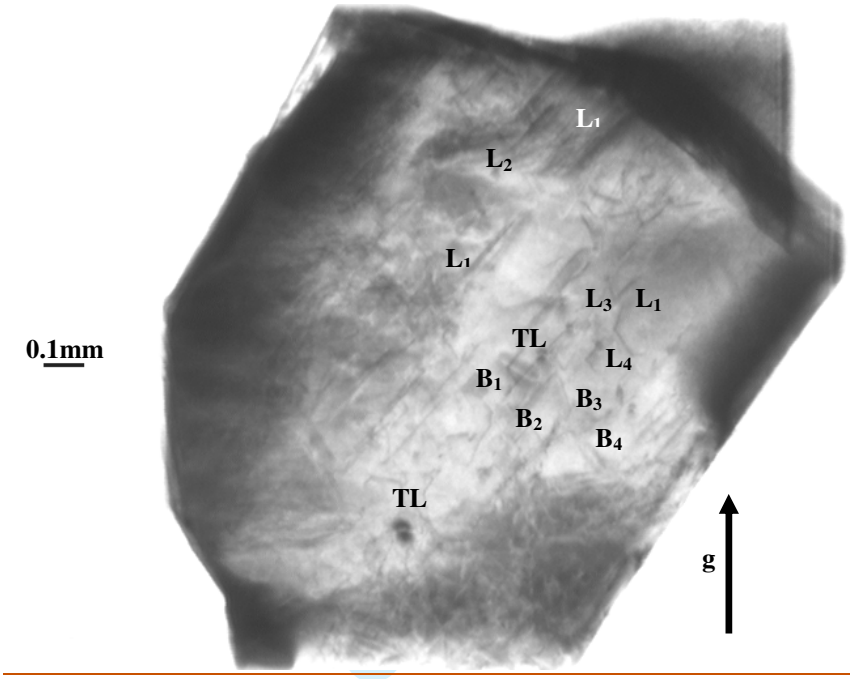

Figure 1

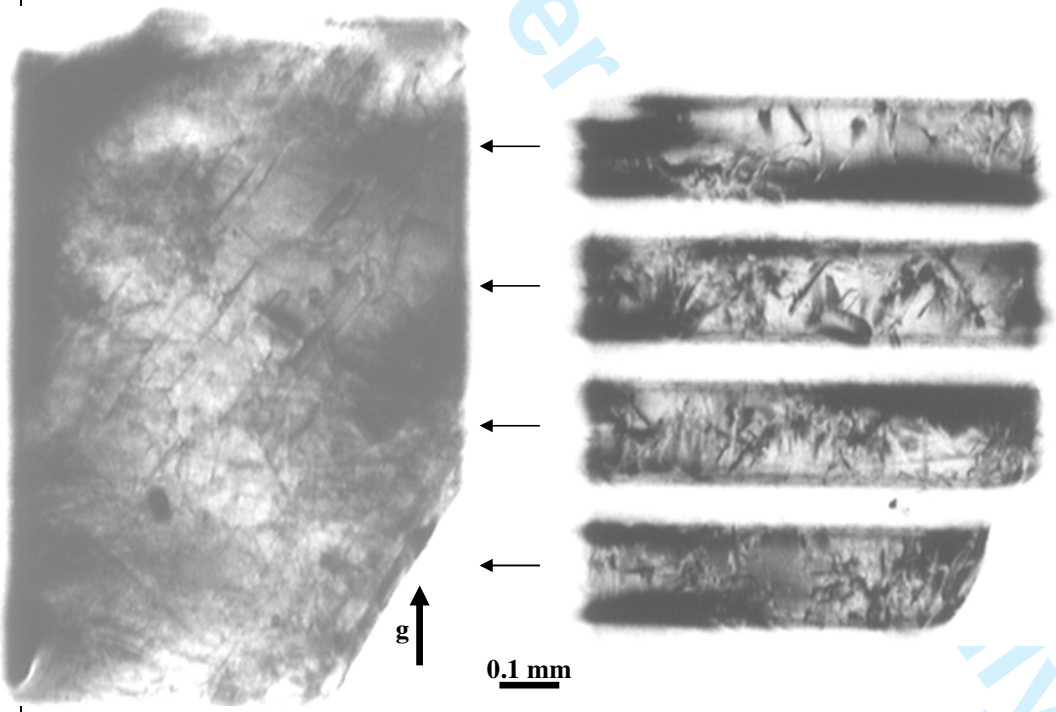

(a) (b)

Figure 2

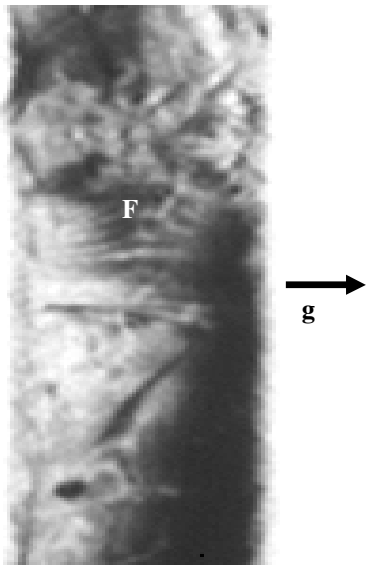

Figure 3

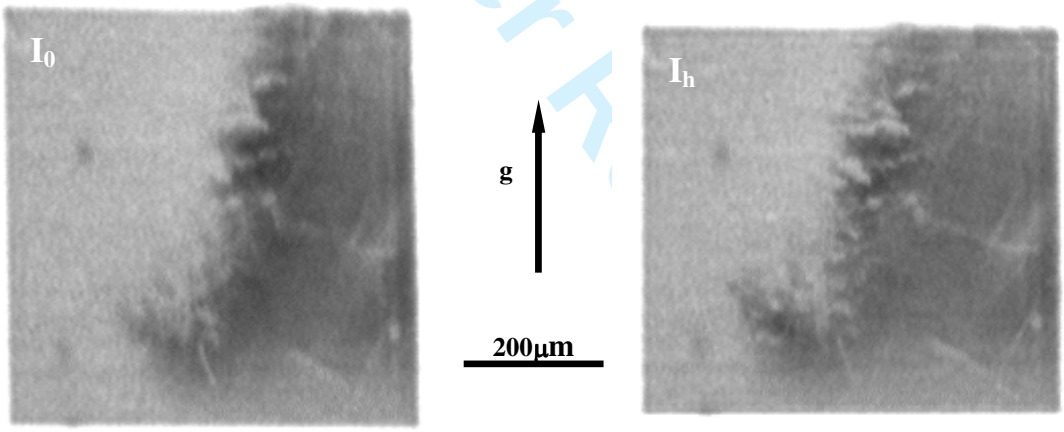

(a) (b)

Figure 4

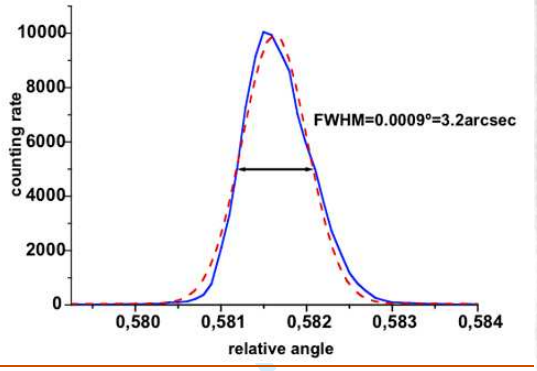

(a)

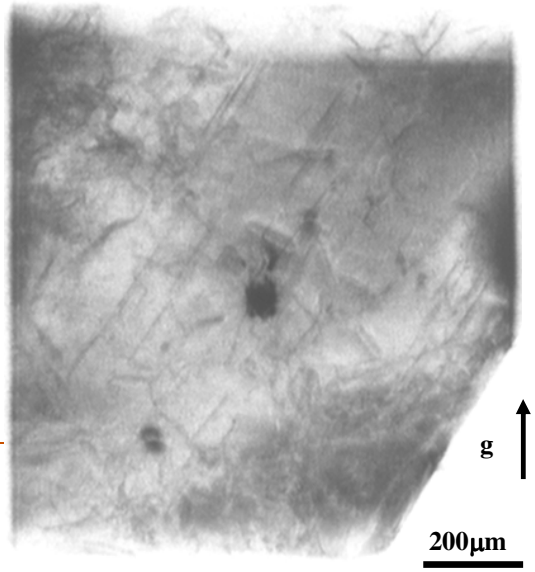

(b)

Figure 5

Formatted: Left

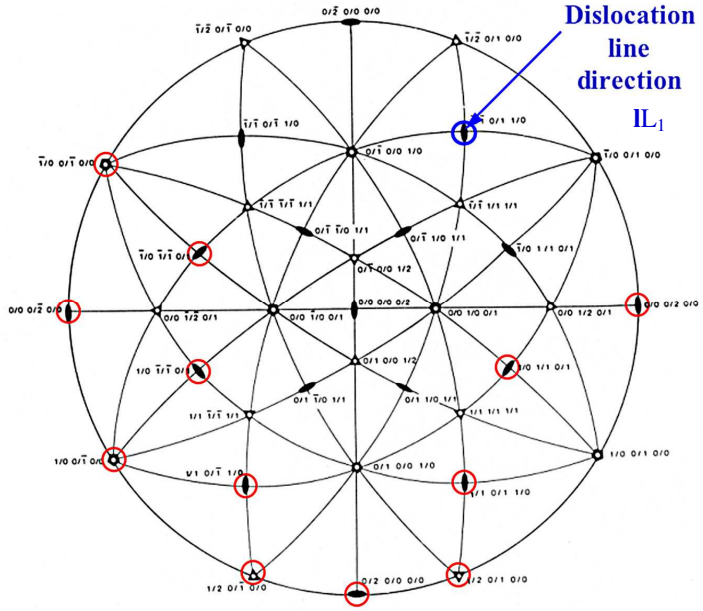

Figure 6

FIGURE CAPTIONS:

Figure 1: Synchrotron monochromatic X-ray topograph recorded from the whole studied grain by rocking it through the Bragg angle by an amount of 0.05°. TL Two-Lobes contrasts, L_i, B_i linear and band contrasts. λ=0.516Å, **g** = τ^2(0/2 0/0 0/0).

Figure 2: Synchrotron monochromatic X-ray topographs recorded from the central region of the studied grain. λ=0.516Å, g = τ^3(0/2 0/0 0/0), rocking angle 0.025°. a) extended beam topograph. b) section topographs, recorded at the level of the arrows using a beam width limited to 20μm in the vertical direction, which are thereby true optical cuts of the grain.

Figure 3 Synchrotron monochromatic X-ray section topograph displaying a set of fringes F. Rocking angle 0.09°, λ=0.516Å, **g** = τ^3(0/0 0/2 0/0).

Figure 4 Synchrotron monochromatic X-ray topographs recorded from a region of 600x600 μm^2 perpendicularly to, a) the forward diffracted beam I_0, b) the diffracted beam I_h. Rocking angle 0.02°, λ=1.033Å, **g** = τ^2(0/2 0/0 0/0).

Figure 5 a) Rocking curve (continuous line) recorded from the region of 50x50 μm^2 marked by a black square in the topograph of figure b and its Gaussian fit (dotted line). b) Synchrotron monochromatic X-ray topograph recorded from a region of 1x1 mm^2. Rocking angle 0.025°, λ=0.516Å, **g** = τ^2(0/2 0/0 0/0).

Figure 6 Stereographic projection of the studied grain showing the directions of respectively, the incident beam (along [0/0 0/0 0/1]), the 12 diffraction vectors $\mathbf{g}_i$ used (red circled) and the lines of contrasts L_1.